Evolution of superconductivity in electron-doped cuprates: Magneto-Raman spectroscopy

M. M. Qazilbash,[1,2,*] A. Koitzsch,[1,†] B. S. Dennis,[1] A. Gozar,[1,‡] Hamza Balci,[2] C. A. Kendziora,[3] R. L. Greene,[2] and G. Blumberg[1,§]

[1]*Bell Laboratories, Lucent Technologies, Murray Hill, New Jersey 07974, USA*

[2]*Center for Superconductivity Research, Department of Physics, University of Maryland, College Park, Maryland 20742, USA*

[3]*United States Naval Research Laboratory, Code 6365, Washington D.C. 20375, USA*

(Received 5 October 2005; published 13 December 2005)

The electron-doped cuprates $Pr_{2-x}Ce_xCuO_{4-\delta}$ and $Nd_{2-x}Ce_xCuO_{4-\delta}$ have been studied by electronic Raman spectroscopy across the entire region of the superconducting (SC) phase diagram. The SC pairing strength is found to be consistent with a weak-coupling regime except in the underdoped region where we observe an in-gap collective mode at $4.5k_BT_c$ while the maximum amplitude of the SC gap is $\approx 8k_BT_c$. In the normal state, doped carriers divide into coherent quasiparticles (QPs) and carriers that remain incoherent. The coherent QPs mainly reside in the vicinity of $(\pm\pi/2a, \pm\pi/2a)$ regions of the Brillouin zone (BZ). We find that only coherent QPs contribute to the superfluid density in the B_{2g} channel. The persistence of SC coherence peaks in the B_{2g} channel for all dopings implies that superconductivity is mainly governed by interactions between the holelike coherent QPs in the vicinity of $(\pm\pi/2a, \pm\pi/2a)$ regions of the BZ. We establish that superconductivity in the electron-doped cuprates occurs primarily due to pairing and condensation of holelike carriers. We have also studied the excitations across the SC gap by Raman spectroscopy as a function of temperature (T) and magnetic field (H) for several different cerium dopings (x). Effective upper critical field lines $H^*_{c2}(T,x)$ at which the superfluid stiffness vanishes and $H^{2\Delta}_{c2}(T,x)$ at which the SC gap amplitude is suppressed by fields have been determined; $H^{2\Delta}_{c2}(T,x)$ is larger than $H^*_{c2}(T,x)$ for all doping concentrations. The difference between the two quantities suggests the presence of phase fluctuations that increase for $x \lesssim 0.15$. It is found that the magnetic field suppresses the magnitude of the SC gap linearly at surprisingly small fields.

DOI: 10.1103/PhysRevB.72.214510 PACS number(s): 74.72.Jt, 74.25.Gz, 74.25.Ha, 78.30.−j

I. INTRODUCTION

The electron-doped (*n*-doped) superconducting (SC) cuprates are an important component in the puzzle of high-T_c superconductivity. There is evidence from transport measurements for both electronlike and holelike carriers in the *n*-doped cuprates $Pr_{2-x}Ce_xCuO_{4-\delta}$ (PCCO) and $Nd_{2-x}Ce_xCuO_{4-\delta}$ (NCCO) for Ce dopings in the vicinity of $x=0.15$.[1–6] Subsequently, angle-resolved photoemission spectroscopy (ARPES) data displayed in Figs. 1(a)–1(c) showed that well-defined electronlike Fermi surface (FS) pockets exist near the $(\pm\pi/4a, \pm\pi/a)$ and $(\pm\pi/a, \pm\pi/4a)$ regions of the Brillouin zone (BZ) for Ce dopings of $0.10 \leqslant x \leqslant 0.15$.[7,8] For $x=0.13$, the ARPES intensity map reveals emergence of a holelike FS around $(\pm\pi/2a, \pm\pi/2a)$ regions of the BZ whose spectral weight increases for $x=0.15$. The Ce doping at which the onset of superconductivity in the underdoped side of the phase diagram is observed approximately coincides with the appearance of the holelike FS seen by ARPES. However, the question of whether one or both electronlike and holelike carriers are responsible for superconductivity has remained unresolved. Despite the fact that conduction and superconductivity occur in the copper-oxygen planes in both the *n*-doped and hole-doped (*p*-doped) cuprates, there are lingering differences in properties between the two types of cuprates that require further investigation if one is to arrive at a comprehensive and unified understanding of the electronic properties of these materials.

While the magnitude and symmetry of the SC order parameter (or SC gap) have been thoroughly studied and understood in the *p*-doped cuprates,[9–11] similar studies have yet to reach a consensus in the optimally doped *n*-doped counterparts. Moreover, there is disagreement among the experiments that have studied the doping dependence of the SC order parameter and superfluid density in the *n*-doped cuprates.[12–16] As far as the distribution of doped carriers is concerned, ARPES at optimal doping above T_c indicates the presence of defined quasiparticles (QPs) and ill-defined incoherent background.[7,17] However, there is a lack of clear understanding of the relationship between the coherence properties of introduced carriers and development of the SC order parameter with doping.

Enhanced temperatures and magnetic fields are known to be detrimental to superconductivity. The effect of temperature on the SC order parameter and superfluid density in the high-T_c cuprate superconductors is extensively documented. However, the influence of the magnetic field on these SC properties at temperatures well below T_c has rarely been investigated spectroscopically, especially for *n*-doped cuprates. Most studies on the *n*-doped cuprates have concentrated on the effect of magnetic field on transport properties.[1–6,18–22] On the theoretical side, researchers have mainly focused on explaining the effects of temperature on SC properties.[23,24] Spectroscopic experiments, as well as theoretical frameworks are necessary for understanding fundamental properties of high-T_c superconductors in magnetic fields. These properties are also critical to SC applications.

Here we report a systematic low energy electronic Raman spectroscopy study of $Pr_{2-x}Ce_xCuO_{4-\delta}$ and $Nd_{2-x}Ce_xCuO_{4-\delta}$ single crystals and films with different cerium dopings covering the entire SC region of the phase diagram and deter-

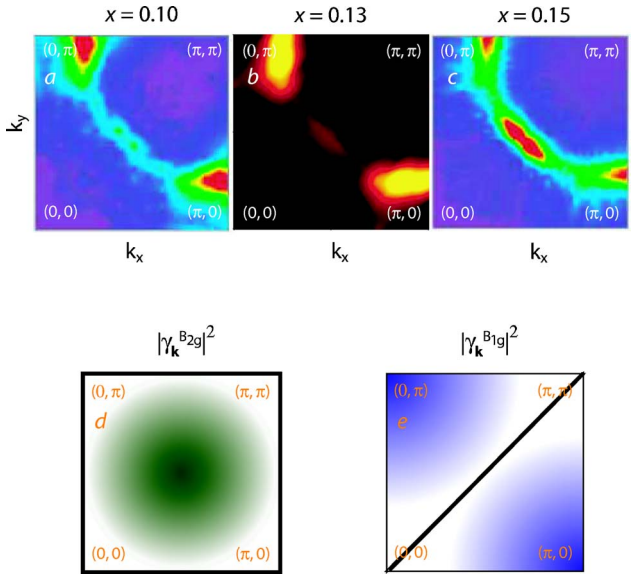

FIG. 1. (Color online) Panels (a)–(c): ARPES intensity for $Nd_{2-x}Ce_xCuO_{4-\delta}$ near the Fermi energy are reproduced from Ref. 7 (a) and (c) and Ref. 8 (b). Evolution of holelike FS near $(\pi/2a, \pi/2a)$ and electronlike FS near $(\pi/4a, \pi/a)$ and $(\pi/a, \pi/4a)$ regions of the BZ with Ce doping (x) are shown. Panels (d) and (e) represent momentum dependence of the Raman coupling $|\gamma_{\mathbf{k}}^{(is)}|^2$ in the B_{2g} and B_{1g} channels, respectively. The regions of the Brillouin zone that contribute to the Raman response in the respective symmetry channels are shaded. The nodes (regions of zero coupling) in corresponding symmetry channels are shown in bold lines.

mine the magnitude of the order parameter as a function of doping. We find that the n-doped cuprates are in the d-wave weak-coupling regime for Ce dopings greater than or equal to optimal doping. The underdoped sample is in the strong-coupling regime and we observe an in-gap collective mode due to strong final state interactions. We establish that the pairing of coherent holelike carriers near $(\pm\pi/2a, \pm\pi/2a)$ regions of the BZ leads to superconductivity in the n-doped cuprates. We also compare the coherent part of the "Raman conductivities" (Refs. 25 and 26) above and below T_c. We show that a weighted superfluid density can be extracted from the SC coherence peaks normalized to the frequency shifts. We find that only coherent QPs contribute to the superfluid density. Moreover, we study the influence of the magnetic field and temperature on quasiparticle excitations across the SC gap directly by a spectroscopic method. We plot the variation of the SC gap and weighted superfluid density as a function of the field. We also extract upper critical field lines $H_{c2}^{*}(T,x)$ at which the superfluid stiffness vanishes and $H_{c2}^{2\Delta}(T,x)$ at which the SC amplitude is suppressed by the field. We find a rapid linear suppression of the SC gap with the field.

II. EXPERIMENTAL METHODS

Raman scattering was performed from natural ab surfaces of single crystals and films of PCCO and single crystals of NCCO. Crystals with different Ce dopings were grown using a flux method.[27] After growth, the crystals were annealed in an Ar-rich atmosphere to induce superconductivity. The SC transitions were measured by a superconducting quantum interference device (SQUID) magnetometer . The Ce concentration of the crystals was measured with x-ray wavelength dispersion spectroscopy. c-axis oriented PCCO films were grown on strontium titanate substrates using pulsed laser deposition.[28,29] The films were grown to a thickness of about 0.8 to 1 μm to minimize the substrate contribution to the Raman signal. The SC transitions were measured by ac susceptibility. Rutherford Backscattering on the films reveals that these thick films are epitaxial and highly oriented. The films provide an opportunity of studying the extremes of the SC phase because of the better control of Ce doping in underdoped and highly overdoped samples.[28,29] Numerous previous studies have established that the phase diagram, crystal structure, and electronic properties of PCCO and NCCO are very similar.

The samples were mounted in an optical continuous helium flow cryostat. The study of polarization dependence of the Raman spectra in zero magnetic field was performed in the pseudobackscattering geometry with linearly polarized 647 and 799 nm excitations from a Kr^+ laser. Incident laser powers between 0.5 and 4 mW were focused to a 50×100 μm spot on the sample surface. For measurements in a magnetic field, the samples were mounted in an optical continuous helium flow cryostat which was inserted into the bore of a superconducting magnet. The magnetic field was applied normal to the ab plane of the samples (i.e., along the c axis of the samples). Raman spectra were measured in a direct backscattering geometry with an incident wavelength of 647 nm. Incident laser powers between 0.5 and 1 mW were focused to a 50 μm diameter spot on the sample surface. The measurements in a magnetic field were performed with circularly polarized light. The spectra displayed in this manuscript were measured at temperatures between 4 and 30 K by a custom triple grating spectrometer and the data were corrected for instrumental spectral response. The sample temperatures quoted in this work have been corrected for laser heating.

III. RAMAN SCATTERING SYMMETRIES

The polarization directions of the incident, $\mathbf{e}_i$, and scattered, $\mathbf{e}_s$, photons are indicated by $(\mathbf{e}_i\mathbf{e}_s)$ with $x=[100]$, $y=[010]$, $x'=[110]$, $y'=[\bar{1}10]$, $R=x+iy$, and $L=x-iy$. The data were obtained in (xy), $(x'y')$, (xx), (RR), and (RL) scattering geometries. For the tetragonal D_{4h} symmetry of the n-doped cuprates, these geometries correspond to $B_{2g}+A_{2g}$, $B_{1g}+A_{2g}$, $A_{1g}+B_{1g}$, $A_{1g}+A_{2g}$, and $B_{1g}+B_{2g}$ representations. Using circularly polarized light we confirmed that the contribution to the A_{2g} channel is very weak for both PCCO and NCCO. The spectra in $(x'y')$ scattering geometry were subtracted from the spectra in the (xx) scattering geometry to obtain the A_{1g} Raman response.

The electronic Raman response function $\chi''^{(is)}(\omega)$ for a given polarization geometry $(\mathbf{e}_i\mathbf{e}_s)$ is proportional to the sum

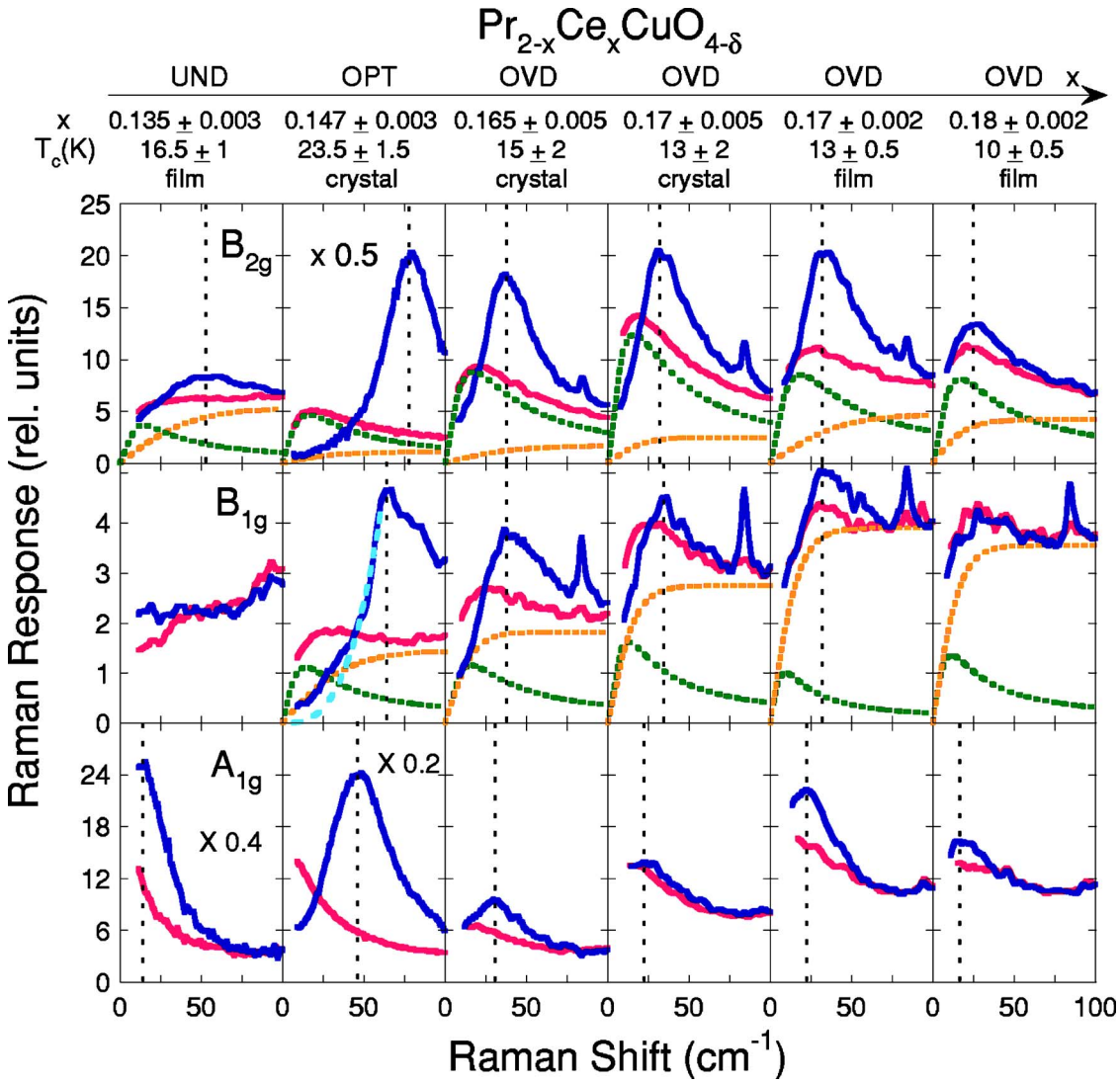

FIG. 2. (Color online) Doping dependence of the low energy electronic Raman response of PCCO single crystals and films for B_{2g}, B_{1g}, and A_{1g} channels obtained with 647 nm excitation. The columns are arranged from left to right in order of increasing cerium doping. Abbreviations UND, OPT, and OVD refer to underdoped, optimally doped, and overdoped samples, respectively. The red (gray) solid curves are the data taken just above the respective T_c of the samples. The normal state response in the B_{2g} and B_{1g} channels is decomposed into a coherent Drude contribution depicted by green (dark gray) dotted lines and an incoherent continuum shown by yellow (light gray) dotted lines. The dark blue (black) solid curves show the data taken in the SC state at $T \approx 4$ K. The dotted vertical lines indicate positions of the SC coherence peaks. For the optimally doped crystal, a low-frequency ω^3 power law is shown by a light blue (light gray) dashed line in the B_{1g} panel for comparison. Overdoped crystals and films show similar behavior, indicating the good quality of the films.

over the density of states at the FS weighted by the square of the momentum ($\mathbf{k}$) dependent Raman vertex $\gamma_{\mathbf{k}}^{(is)}$.[30–33] Because the scattering geometries selectively discriminate between different regions of the FS, electronic Raman spectroscopy provides information about both the magnitude and the $\mathbf{k}$ dependence of the SC OP. In the effective mass approximation $\gamma_{\mathbf{k}}^{B_{1g}} \propto t(\cos k_x a - \cos k_y a)$ and $\gamma_{\mathbf{k}}^{B_{2g}} \propto 4t'(\sin k_x a \sin k_y a)$ where t and t' are nearest and next-nearest-neighbor hopping integrals in the tight-binding model. For the B_{2g} channel, the Raman vertex is most sensitive to $(\pm\pi/2a, \pm\pi/2a)$ regions of the BZ and vanishes along $(0,0) \rightarrow (\pi/a, 0)$ and equivalent lines. For the B_{1g} channel, nodal $(0,0) \rightarrow (\pi/a, \pi/a)$ diagonals do not contribute to the intensity that mainly integrates from regions near intersections of the FS and the BZ boundary. The pictorial representations of the B_{2g} and B_{1g} channels are shown in Figs. 1(d) and 1(e). On comparison with ARPES data, one can see that the B_{2g} scattering channel probes the holelike pockets in the vicinity of the $(\pm\pi/2a, \pm\pi/2a)$ regions of the BZ while Raman intensity in the B_{1g} channel originates from the electronlike FS near the $(\pm\pi/4a, \pm\pi/a)$ and $(\pm\pi/a, \pm\pi/4a)$ regions of the BZ. The unscreened Raman response in the A_{1g} channel does not have symmetry imposed nodal lines and measures an overall average throughout the BZ. However, the full symmetric response is expected to be screened by Coulomb-interaction-induced charge backflow that redistributes and strongly suppresses the spectral intensity. The screening is expected to be weaker

if the Raman vertex $\gamma_{\mathbf{k}}^{A_{1g}}$ is rapidly changing with the wave vector.[34]

IV. DOPING AND POLARIZATION DEPENDENCE

In Fig. 2 we show doping dependence of the low energy electronic Raman response of PCCO single crystals and films. One can see that the Raman scattering intensity is significantly stronger in the B_{2g} than in the B_{1g} channel for all Ce concentrations. This is only partly due to resonance resulting from interband transitions.[35] More importantly, it underlines the significance of next-nearest-neighbor hopping t' in n-doped cuprates and is in contrast with p-doped cuprates where the response in the B_{2g} channel is generally weaker than in B_{1g}.[36] Coulomb screening should lead to a much weaker Raman response in the fully symmetric A_{1g} channel. However, we find that the intensities in the A_{1g} channel are of the same order of magnitude as those in the nonsymmetric B_{1g} and B_{2g} channels in the overdoped samples and are significantly stronger in the under- and optimally-doped samples. This lack of screening is possible if the effective mass on the FS changes sign.[37] This is the case in the electron-doped cuprates where strong evidence exists for both electronlike and holelike carriers.[1–3,6–8]

We decompose the Raman response in the normal state into two parts, a featureless continuum and a low-frequency quasielastic scattering peak (QEP):

$$\chi_N''(\omega) = \chi_{QEP}''(\omega) + \chi_{MFL}''(\omega). \tag{1}$$

The QEP response

$$\chi_{QEP}''(\omega) = a^{(is)} \frac{\Gamma\omega}{\omega^2 + \Gamma^2} \tag{2}$$

is described in a Drude model as QP contribution from doped carriers[26,38] while the featureless continuum

$$\chi_{MFL}''(\omega) = b^{(is)} \tanh(\omega/\omega_c) \tag{3}$$

represents a collective incoherent response.[39] Symmetry-dependent $a^{(is)}$ and $b^{(is)}$ parameters control the spectral weight in these coherent and incoherent channels, ω_c is a cutoff frequency of order k_BT (Ref. 39), and the QEP position Γ is the Drude scattering rate that at low temperatures is about 2 meV for the entire doping range studied. The Drude part describes the relaxation dynamics of the QPs that results from electron-electron interactions and is, therefore, strongly temperature dependent[38] in contrast to scattering from impurities which is expected to be independent of temperature. This deconvolution of the Raman response into two components presented here is consistent with the ARPES data that display defined QPs as well as ill-defined excitations in different parts of the FS.[7,17] One can observe from the deconvolution that the Raman response in the B_{2g} channel is dominated by the QP (Drude) response while the B_{1g} channel is dominated by the incoherent continuum.[40] The well-defined holelike QP states reside mainly in the vicinity of the $(\pm\pi/2a, \pm\pi/2a)$ regions of the BZ. The evolution of the integrated QP spectral weight of the "Raman conductivity" (Refs. 25 and 26)

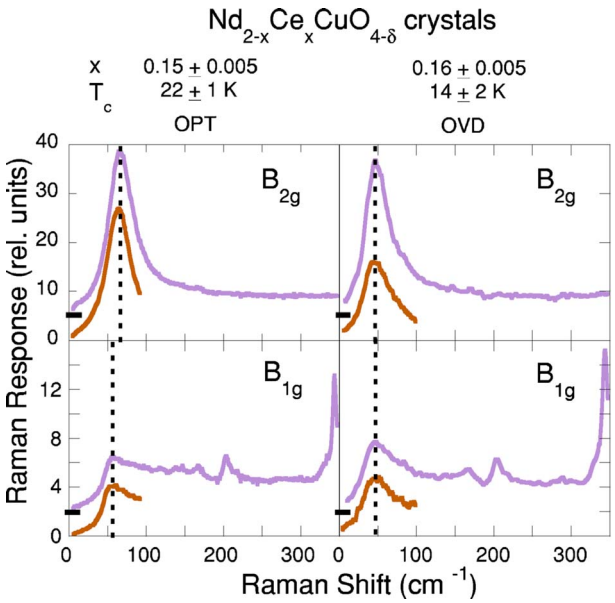

FIG. 3. (Color online) A comparison of the Raman response in the superconducting state for an optimally doped (OPT) NCCO crystal in the first column and an over-doped (OVD) NCCO crystal in the second column. The first and second rows show spectra for B_{2g} and B_{1g} channels respectively. The violet (light grey) and brown (dark grey) curves are data taken with red laser excitation (λ_L =647 nm) and near-IR excitation (λ_L=799 nm). The B_{2g} and B_{1g} data for λ_L=647 nm has been shifted up by 5 units and 2 units respectively. All spectra are taken at $T \approx 4$ K. The dotted vertical lines show the positions of the SC coherence peaks. Data with near-IR laser excitation was obtained up to 100 cm^{-1} Raman shift.

$$I_N^{B_{2g}}(x) = \int (\chi_{QEP}''^{B_{2g}}/\omega) d\omega \tag{4}$$

as a function of Ce doping x is shown in Fig. 4(c). While on the underdoped side, $I_N^{B_{2g}}(x)$ exhibits the expected increase proportional to x, the integrated coherent contribution saturates above optimal doping $x \gtrsim 0.145$. At higher Ce doping, additional carriers contribute mainly to the electronlike incoherent response and can be observed as an increasing intensity of the featureless Raman continuum $\chi''_{\mathrm{MFL}}(\omega)$, particularly in the B_{1g} channel.

V. PAIR BREAKING EXCITATIONS

In the SC state, the strength of the low-frequency intensity in the normal state is reduced and the spectral weight moves to the 2Δ coherence peak resulting from excitations out of the SC condensate. In the B_{2g} and A_{1g} channels, the "pair-breaking" SC coherence peaks appear for all dopings while in the B_{1g} channel these SC coherence peaks are negligibly weak in the underdoped and the most overdoped films. For the optimally doped crystal (T_c=23.5 K), the SC coherence peak energy is larger in the B_{2g} channel compared with that in B_{1g}, and for all channels it is larger than the scattering rate Γ obtained from the spectra in the normal state. The intensity below the SC coherence peaks vanishes smoothly without a threshold to the lowest frequency measured. The absence of

a threshold that has been observed in *s*-wave superconductors precludes interpretation in terms of a fully gapped FS.[30,31] The smooth decrease in the Raman response below the SC coherence peak is consistent with nodes in the gap. We compare the low-frequency tail in the B_{1g} response (Fig. 2) to an ω^3 power law that is expected for a $d_{x^2-y^2}$-wave superconductor in the clean limit.[41] The observed deviation from a cubic to a linear response at the lowest frequencies is an indication of low-energy QP scattering.[42] The data for optimally doped PCCO are very similar to that for optimally doped NCCO (see Fig. 3) which was interpreted in terms of a nonmonotonic *d*-wave order parameter with nodes along the $(0,0)\rightarrow(\pi/a,\pi/a)$ diagonal and the maximum gap being closer to this diagonal than to the BZ boundaries.[35] Recent evidence from ARPES that the SC gap maximum is located closer to the nodal direction in optimally doped samples confirms the interpretation of the Raman data.[43]

Interestingly, in the overdoped PCCO samples (Fig. 2) and overdoped NCCO crystal samples (Fig. 3), the SC coherence peak positions are at the same energies for both the B_{2g} and B_{1g} channels. The peak positions and intensities decrease in the overdoped regime compared to the optimally doped samples. Moreover, the peak energies are similar to Γ indicating that superconductivity is departing from the clean limit.[42] The Raman response below the SC coherence peaks vanishes smoothly and no well-defined threshold is observed. The data for the 799 nm excitation are measured down to 4.5 cm^{-1} and shows no obvious subgap threshold. The peak positions and the subgap Raman response in the NCCO crystals are almost independent of the laser excitation energies (Fig. 3). Similar symmetry-independent pair-breaking peak energies with continuously decreasing Raman scattering intensity down to low frequencies have been observed in the Raman spectra in overdoped samples of *p*-doped Bi-2212.[44–46] The Raman data presented in Figs. 2 and 3 for overdoped *n*-doped samples is similar to the Raman data for overdoped Bi-2212. The coincidence of coherence peak energies in the B_{1g} and B_{2g} channels may be caused by enhanced QP scattering,[42] although this remains an open question. Nevertheless, the smooth and continuous decrease in Raman intensity below the coherence peak is consistent with a nodal gap structure.[15,16]

In Fig. 4(a) we show that the SC coherence peak energy (2Δ) has a pronounced maximum at optimal doping. For comparison, we include the value of twice the SC gap energy obtained from point contact tunneling spectroscopy.[12,47] For optimally and overdoped samples the maximum values of the Raman SC coherence peak energies are very similar to the single particle spectroscopy gap values and can, therefore, be associated with twice the SC gap magnitude. This is not the case for underdoped samples where the tunneling spectroscopy data exhibit a gap (2Δ) that is larger than the Raman SC coherence peak energy of 52 cm^{-1} ($\approx$6.4 meV). The normalized tunneling gap value in Fig. 4(b) suggests that the underdoped *n*-doped cuprates are in the strong-coupling regime. Therefore, in underdoped samples the two QPs excited out of the SC condensate by Raman processes continue to interact, binding into a collective excitonic state that costs less energy than excitation of two independent

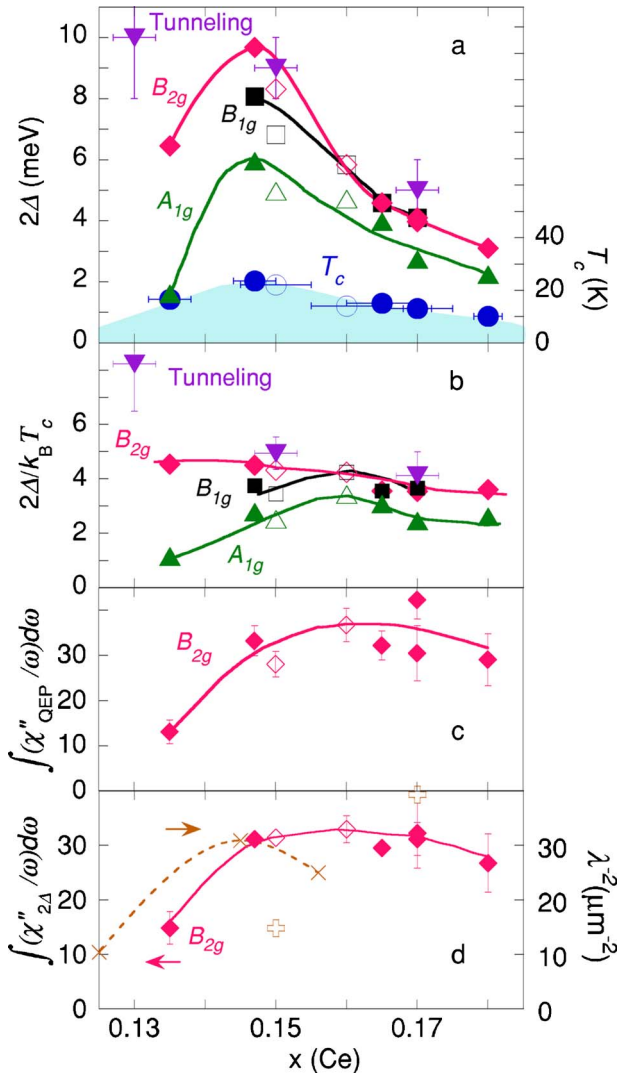

FIG. 4. (Color online) The phase diagram of PCCO (filled symbols) and NCCO (open symbols) superconductors explored by Raman spectroscopy. Panels show: (a) T_c (circles) and 2Δ peak positions for three Raman channels B_{1g} (squares), B_{2g} (diamonds), and A_{1g} (upright triangles) as well as the separation between coherence peaks from point contact tunneling spectroscopy (inverted triangles); (Refs. 12 and 47) (b) magnitude of the normalized SC coherence peaks ($2\Delta/k_BT_c$) from three Raman channels, and from tunneling; (Refs. 12 and 47) (c) the integrated quasiparticle (Drude) response just above T_c; (d) integrated intensity of reduced 2Δ coherence peaks ($\chi''_{2\Delta}/\omega$) at 4 K. For comparison, we plot $1/\lambda(0)^2$ values from Ref. 13 ($\times$) and Ref. 15 (open crosses). Error bars on the cerium concentrations are shown only on the T_c data points to preserve clarity of the figure. Solid and dashed lines are guides to the eye.

QPs. The SC coherence peak in the B_{2g} channel in the underdoped sample is actually an in-gap collective mode. Similar observations were made previously in the *p*-doped cuprates in the B_{1g} channel.[36,48,49] The significance of final state interactions in the formation of a collective mode in underdoped *p*-doped cuprates has been demonstrated in Refs. 50–52. The important difference here is that in the *n*-doped cuprates the collective mode appears in the B_{2g} channel.

We note for the $x=0.13$ sample the first appearance of the SC coherence peak in the B_{2g} channel coincides with the appearance of a holelike FS near the $(\pm\pi/2a, \pm\pi/2a)$ regions of the BZ as viewed by ARPES [see Fig. 1(b) and Ref. 8] while the response in the B_{1g} channel does not show any comparable signatures of superconductivity. These observations relate superconductivity to the appearance of the holelike FS. The electronlike carriers that are clearly present near the $(\pm\pi/4a, \pm\pi/a)$ and $(\pm\pi/a, \pm\pi/4a)$ regions of the FS do not show contribution to superconducting pairing. When Ce doping is increased to $x\approx0.15$, ARPES data show that the electron pocket persists and the excitations around holelike FS acquires more coherent spectral weight.[7] Well-defined SC coherence peaks appear in both B_{2g} and B_{1g} channels with the peak energy about 20% higher in the B_{2g} channel. One can infer that for optimal doping the superconductivity exists in both hole and electron bands but the gap is larger in the hole channel. For overdoped samples, it is likely that the FS is holelike and centered at $(\pm\pi/a, \pm\pi/a)$ points. The evolutionary trend of the FS with doping in the ARPES data supports this view though ARPES data on overdoped samples are still lacking. The situation may be more complicated because there is evidence from Hall effect data that both holelike and electronlike carriers exist even for overdoped samples with $x=0.17$.[3,6] Nevertheless, holelike carriers dominate the low temperature Hall effect data for dopings $x\geqslant0.16$. Therefore, one can hypothesize that in the overdoped samples, condensation of holelike carriers is primarily responsible for the SC coherence peaks in all Raman scattering symmetries.

Reduced energies of the Raman SC coherence peaks, $2\Delta/k_BT_c$, are plotted in Fig. 4(b) as a function of doping. For the channel that exhibits the highest ratio, B_{2g}, the values fall between 4.5 for the optimally doped samples and 3.5 for the most over doped samples. These ratios are consistent with those inferred from electron tunneling and infrared reflectivity measurements,[12,47,53] and within the prediction of the mean-field BCS values for *d*-wave superconductors.[24] The coherence peak energy remains below $4.2k_BT_c$ for the B_{1g} channel and is even lower for the A_{1g} channel. The reduced energies for all the channels are lower than for *p*-doped materials[36,48,49,54] suggesting a *d*-wave BCS weak-coupling limit in the *n*-doped cuprates for optimally and overdoped samples.

VI. RAMAN SUM RULE

In Fig. 4(d) we plot the integrated reduced coherence peak intensity in the SC state,

$$I_{SC}^{B_{2g}}(x) = \int (\chi''^{B_{2g}}_{2\Delta}/\omega)d\omega, \tag{5}$$

where $\chi''^{B_{2g}}_{2\Delta}(\omega)$ is the SC coherence response with the incoherent continuum subtracted. The details of the analysis are given in the Appendix. For the nonsymmetric channels in $T\rightarrow0$ limit

$$I_{SC}^{(is)} \propto \sum_{\mathbf{k}} (\gamma_{\mathbf{k}}^{(is)})^2 \frac{{\Delta_{\mathbf{k}}}^2}{2{E_{\mathbf{k}}}^3} \tag{6}$$

is proportional to the superfluid density

$$\rho_s \propto \sum_{\mathbf{k}} \frac{{\Delta_{\mathbf{k}}}^2}{2{E_{\mathbf{k}}}^3} \tag{7}$$

weighted by the square of the Raman coupling vertex.[24,55] Here $E_{\mathbf{k}}$ is the QP dispersion in the SC state and $\Delta_{\mathbf{k}}$ is the SC gap. The superfluid densities ($\rho_s\propto1/\lambda^2$) obtained from penetration depth (λ) measurements[13,15] are plotted in Fig. 4(d) for comparison.[56] We note that the values of the integrated reduced coherence intensities in the B_{2g} channel do not change from the normal to the SC state [Figs. 4(c) and 4(d)] demonstrating a partial sum rule similar to the Ferrell-Glover-Tinkham sum rule in optics. Also, the $I_N^{B_{2g}}(x) = I_{SC}^{B_{2g}}(x)$ equality implies that only Drude QPs control the superfluid density and that the electronlike incoherent carriers doped above optimal doping do not contribute to the superfluid stiffness.

Certain aspects of the observations in the preceding paragraph need further comment. For conventional superconductors that are Fermi liquids above T_c, the theory does not predict a partial sum rule for low energy Raman scattering connecting the normal and SC states akin to the Ferrell-Glover-Tinkham sum rule in optics. However, we have experimentally demonstrated the existence of a partial Raman sum rule at low energies in the normal and SC states for the *n*-doped cuprates. The question of whether this partial sum rule is limited to the *n*-doped cuprates or is more generic encompassing *p*-doped cuprates as well can be decided by a similar analysis of the Raman data that exists for several families of *p*-doped cuprates.

VII. EFFECTS OF TEMPERATURE AND MAGNETIC FIELD

Circularly polarized light in the right-left (RL) scattering geometry was used for the data displayed in this section. For the tetragonal D_{4h} symmetry, this geometry corresponds to the sum of $B_{1g}+B_{2g}$ representations. It has been shown in previous Raman measurements that for the 647 nm incident laser light the scattering in the B_{2g} channel is resonantly enhanced and is about an order of magnitude greater than scattering intensity in the B_{1g} channel.[35] Therefore, the B_{2g} channel dominates the spectra for right-left polarization.

To recap, the QP excitations across the SC gap lead to a pair-breaking 2Δ coherence peak close to twice the gap energy. The 2Δ peak is a measure of the magnitude of the SC order parameter for optimally and overdoped samples, while the integrated intensity of the reduced 2Δ coherence peak

$$I_{SC}(H,T) = \int [\chi''_{2\Delta}(\omega,H,T)/\omega]d\omega \tag{8}$$

is related to the superfluid density ρ_s. This is the framework that forms a basis for analysis of the Raman data in this section.

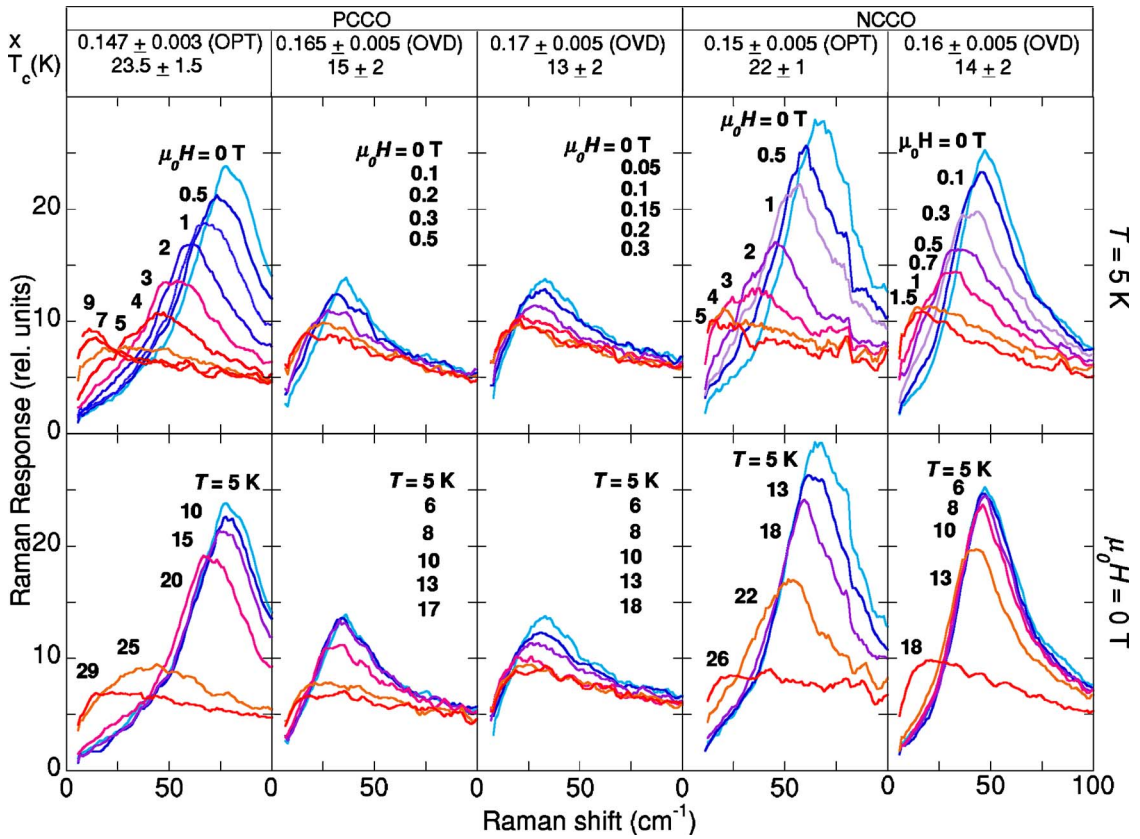

FIG. 5. (Color online) Raman response function $\chi''(\omega,H,T)$ for 647 nm excitation and RL polarization for five single crystals of PCCO and NCCO with different Ce dopings x. Abbreviations OPT and OVD stand for optimally doped and overdoped samples, respectively. The first row shows the disappearance of the 2Δ coherence peak in increasing magnetic field applied normal to the *ab* plane of the crystals at 5 K. The second row shows the temperature dependence of the 2Δ peak in zero magnetic field.

Figure 5 exhibits the field and temperature dependence of the SC coherence peak at the maximum gap value ($2\Delta_{max}$) for the optimally doped ($x \approx 0.15$) and overdoped ($x > 0.15$) PCCO and NCCO crystals. The coherence peak loses intensity and moves to lower energies by either increasing the temperature or magnetic field. We define an effective upper critical field $H^*_{c2}(T,x)$ as the field that completely suppresses the coherence peak intensity: the Raman response remains field independent for $H > H^*_{c2}$. Above T_c or H^*_{c2} the SC coherence peak vanishes and the Raman response acquires a low-frequency QEP. The non-SC response is similar for both cases: $T > T_c$ and $H > H^*_{c2}$ at the lowest temperature, and therefore is independent of the means used to quench superconductivity. As discussed previously, the Raman response in the normal state can be described by a QEP Drude response of doped QP carriers above an incoherent featureless continuum, Eqs. (1)–(3). At low temperatures $\Gamma(x) \approx 2$ meV for the entire studied doping range.

Reduced gap values $2\Delta_{max}/k_BT_c$ from Raman data in zero field on five single crystals of various doping levels are plotted in Fig. 6(a) as a function of the reduced temperature (T/T_c). For the lowest measured temperature $2\Delta_{max}/k_BT_c$ values fall between 4.5 for the optimally doped crystals and 3.5 for the most overdoped PCCO crystals. For optimally doped samples, the gap appears to open up faster than the mean-field BCS prediction[24] as the temperature is reduced below T_c suggesting phase fluctuations and a finite pairing amplitude above T_c. The temperature dependence of the gap energy for the most overdoped samples is close to the prediction of BCS theory.[62]

The mixed state consists of normal regions inside vortex cores coexisting with SC regions surrounding the vortices. The Raman response in a field, $\chi''(\omega,H,T)$, is assumed to be a sum of contributions from the SC and normal regions. The normal state contribution to the measured Raman spectra is further assumed to be proportional to the number of vortices which itself is proportional to the applied field:

$$\chi''(\omega,H,T) = \chi''_{SC}(\omega,H,T) + \frac{H}{H^*_{c2}}\chi''_N(\omega,T). \qquad (9)$$

Here $\chi''_N(\omega,T)$ is the normal state Raman response at or above the critical field value $H^*_{c2}(T)$. We extract the Raman response of the SC regions $\chi''_{SC}(\omega,H,T)$ from the data using Eq. (9). We then decompose $\chi''_{SC}(\omega,H,T)$ into a low-frequency SC 2Δ coherence peak $\chi''_{2\Delta}(\omega,H,T)$ and a featureless continuum above the peak frequency. H^*_{c2} in Eq. (9) is the estimate of the upper critical field at which the SC coherence peak vanishes in the raw data.

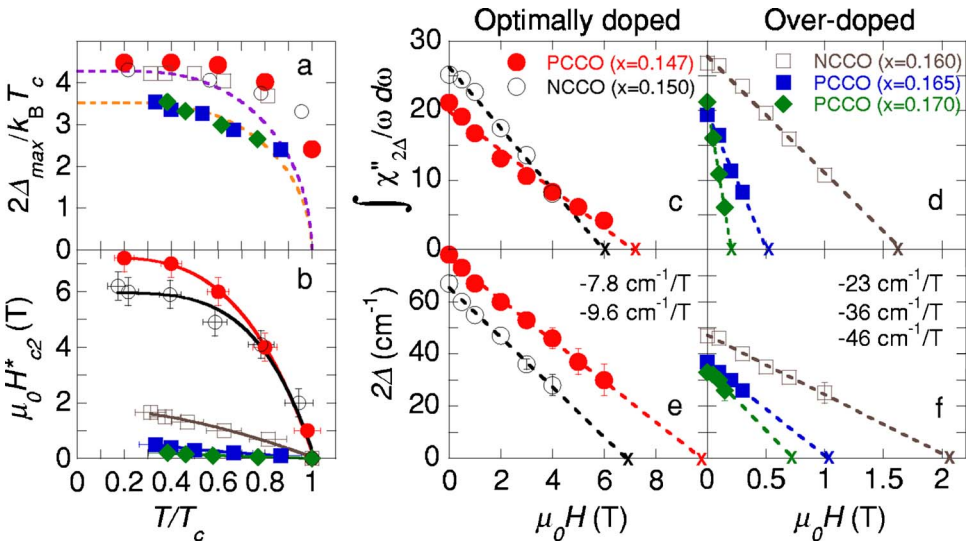

FIG. 6. (Color online) The temperature and field dependence of the SC order parameter amplitude and stiffness for two NCCO (with Ce dopings x=0.15 and 0.16; open symbols) and three PCCO (x=0.147, 0.165 and 0.17; filled symbols) single crystals. The same symbols are used for all plots to indicate data on a particular crystal. The temperature dependence (a) of the reduced SC gap magnitude at zero field, and (b) of the effective upper critical field H^*_{c2} that completely suppresses the SC coherence peak intensity at the given temperature. In plot (a) the dashed lines are weak-coupling BCS predictions for temperature dependence of *d*-wave [violet (dark gray)] and *s*-wave [yellow (light gray)] SC gaps. Horizontal error bars are not shown in (a) and are the same as in (b). Solid lines in (b) are guides to the eye. The field dependence at 5 K of the integrated reduced SC coherence intensity, $I_{SC}(H)$, is shown in panels (c) and (d) and the SC coherence peak energy (2Δ) in panels (e) and (f) for optimally doped and overdoped crystals correspondingly. "x" indicates the effective upper critical fields (H^*_{c2}) and the field values of the SC gap collapse ($H^{2\Delta}_{c2}$) extrapolated from the data. The dashed lines are linear fits to the data. Panels (e) and (f) also include the rate of gap suppression $\partial 2\Delta(H,T)/\partial H$.

VIII. UPPER CRITICAL FIELDS AND SUPERCONDUCTING COHERENCE LENGTH

Estimates of H^*_{c2} for different temperatures and Ce concentrations are plotted vs T/T_c in Fig. 6(b). $H^*_{c2}(T)$ displays negative curvature to the lowest measured temperature (5 K). $H^*_{c2}(T)$ saturates at low temperatures for samples near optimal doping. With increasing doping we observe a dramatic reduction of H^*_{c2} in the entire temperature range.

In Figs. 6(c) and 6(d) we plot for optimally and overdoped crystals, the integrated coherence intensity $I_{SC}(H,T)$ at $T \approx 5$ K, as a function of field. $I_{SC}(H,T)$ is proportional to the superfluid density ρ_s weighted by the square of the Raman coupling vertex [Eqs. (6) and (7)]. In the panels Fig. 6(e) and 6(f) the coherence peak energy $2\Delta(H)$ is displayed as a function of field at $T \approx 5$ K. It appears that both the superfluid stiffness and the SC gap magnitude show a monotonic almost linear decrease with field. We use a linear continuation to determine critical values of H^*_{c2} and $H^{2\Delta}_{c2}$ that completely suppress the superfluid density and amplitude of the SC order parameter correspondingly. H^*_{c2} is thus determined self-consistently and agrees with our initial estimates based on the raw data. We find that the SC gap still remains open at a finite value at the effective critical fields H^*_{c2}. We find that the rate of gap suppression, $\partial 2\Delta(H,T)/\partial H$, is strongly doping dependent: -8 cm^{-1} T^{-1} for the optimally doped crystal rapidly increases with doping to a surprisingly large -46 cm^{-1} T^{-1} for overdoped PCCO with $x=0.17$.

These observations are in sharp contrast to *p*-doped cuprates where the field-induced suppression of the SC coherence peak intensity is not accompanied by any observable shift in the gap magnitude.[59] Moreover, these observations are also different from the weak shift of the SC mode energy with fields in the Raman spectra on $NbSe_2$, a BCS-type *s*-wave superconductor.[60,61] The Doppler shift due to circulating supercurrents cannot explain the rapid suppression of the SC gap magnitude. The rate of change of the Zeeman energy with fields is much less than the observed rate of gap magnitude suppression and can be ruled out as a cause of this suppression. A possible scenario for the rapid reduction of $H^{2\Delta}_{c2}$ with doping is related to the nonmonotonic *d*-wave form of the SC gap in *n*-doped cuprates for which the points of maximum gap amplitudes with opposite phase are close to each other in reciprocal space.[35,43] In this situation, introduction of vortices leads to QP scattering between points of large gap amplitude with opposite phase which is self-damaging for the gap amplitude.

We turn to Fig. 7 where the upper critical fields, $H^*_{c2}(x)$ and $H^{2\Delta}_{c2}(x)$, and the related Ginzburg-Landau SC coherence length $\xi_{GL}(x)=\sqrt{\Phi_0/2\pi H^{2\Delta}_{c2}(x)}$ (Φ_0 is the fluxoid quantum) are plotted vs Ce doping x.[63] The H^*_{c2} value of 7.2 ± 0.5 T for the optimally doped PCCO crystal is in agreement with $H_{c2} \approx 8$ T determined by thermal conductivity[20] and specific heat measurements.[64] This value also agrees with the H_{c2} estimated by tunneling spectroscopy on optimally doped samples.[47,66,67] Nernst effect measurements estimate $H_{c2} \approx 10$ T for optimally doped samples,[19] consistent with $H^{2\Delta}_{c2}=9.7\pm0.5$ T. The SC phase coherence vanishes at a lower critical field while the pairing amplitude persists up to a higher field. This supports our earlier interpretation of the

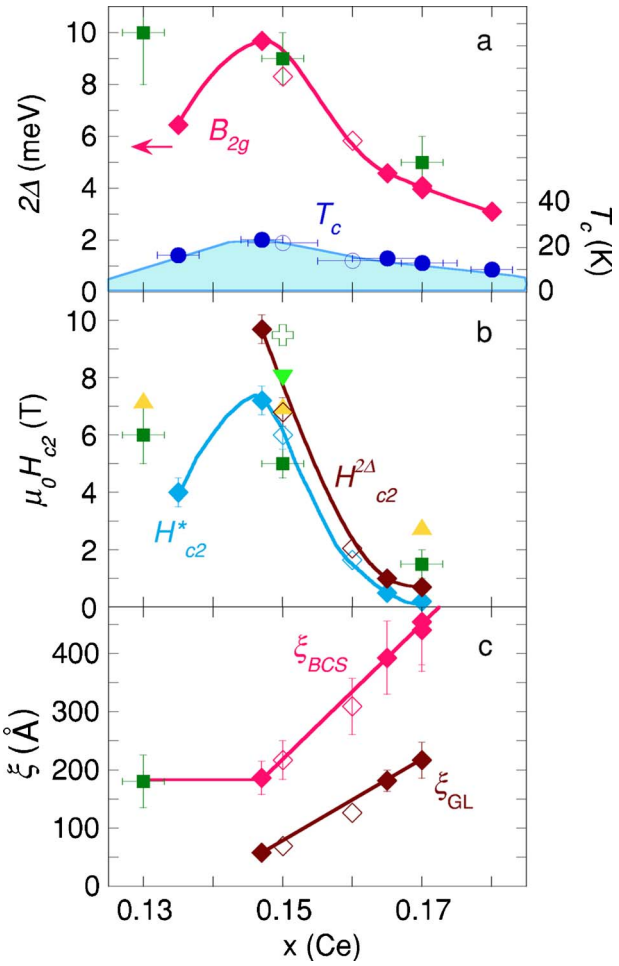

FIG. 7. (Color online) The SC phase diagram of PCCO (filled diamonds) and NCCO (open diamonds) explored by electronic Raman scattering in magnetic field. Panels show: (a) T_c (circles), the maximum energy of the 2Δ peak from Raman spectroscopy (diamonds), and the distance between coherence peaks from point contact tunneling spectroscopy (squares) (Refs. 12 and 47); (b) the doping dependence at 5 K of the effective upper critical fields $H^*_{c2}(x)$ [light blue (light gray) diamonds] and the fields suppressing the gap amplitude $H^{2\Delta}_{c2}(x)$ [brown (dark gray) diamonds] is compared to upper critical fields obtained from other measurements: tunneling spectroscopy (Refs. 47 and 65) (squares), Nernst effect on PCCO films (Ref. 21) (upright triangles), Nernst effect on NCCO crystal (Ref. 19) (cross), and thermal conductivity (Ref. 20) (inverted triangle); (c) the Ginzburg-Landau SC coherence length $\xi_{GL}(x)$ [brown (dark gray) diamonds] is compared to the BCS coherence length $\xi_{BCS}(x)$ [red (light gray) diamonds]. For the underdoped sample, the gap value from point contact tunneling is used to calculate ξ_{BCS} while for all other dopings the gap values in the Raman B_{2g} channel [Fig. 7(a)] have been used. The error bars on the Ce concentrations x are shown only on the T_c data points to preserve clarity of the figure. All solid lines are guides to the eye and are labeled.

temperature dependence of the gap in terms of phase fluctuations above T_c. With increasing doping, $H^{2\Delta}_{c2}$ drops by an order of magnitude reducing to 0.7 T for the $x=0.17$ overdoped PCCO crystal.[68] Correspondingly, $\xi_{GL}(x)$ rapidly increases with doping from 60 Å at optimal doping to 220 Å for $x=0.17$ PCCO.

We note that the H_{c2} value of optimally doped films from magnetoresistivity, using the full recovery of resistivity criterion,[22] is consistent with that obtained from Raman and thermodynamic measurements. However, for the overdoped film ($x\approx 0.17$), H_{c2} (at 5 K) based on the appearance of resistance[22] is consistent with $H^{2\Delta}_{c2}$ from the Raman data on similarly doped crystals. This could mean that vortex flow physics, which plays a dominant role in cuprate superconductors with short coherence lengths, becomes less important in the overdoped n-type cuprates with longer coherence lengths.[69,70]

In Fig. 7(c) we show that the values for $H^{2\Delta}_{c2}(x)$ are related to the SC gap. We compare here $\xi_{GL}(x)$ to the BCS coherence length $\xi_{BCS}(x)=\hbar v_F/\pi\Delta_{max}(x)$, where the Fermi velocity $v_F=4.3\times 10^5$ m/s is estimated from ARPES measurements[71] and the lowest temperature SC gap values $\Delta_{max}(x)$ are used from Raman and tunneling data.[47] The comparison plot reveals that the $\xi_{BCS}(x)$ trend resembles the doping dependence of $\xi_{GL}(x)$ and therefore confirms the relation of $H^{2\Delta}_{c2}(x)$ to the pairing potential $\Delta_{max}(x)$. It also indicates that $\xi_{GL}(x)$ is still about two times lower and $H^{2\Delta}_{c2}(x)$ is about four times higher than expected for a conventional BCS superconductor with a corresponding isotropic gap.

ξ_{GL} for the n-doped cuprates is significantly larger than for their p-doped counterparts and that leads to important differences. First, the size of the Cooper pair is larger than the average interparticle spacing: $k_F\xi_{GL}$ ranges between 40 and 150, still smaller than for conventional BCS superconductors but an order of magnitude larger than for the p-doped cuprates. Second, a larger Cooper pair size requires further pair interactions to be taken into account and leads to a more complicated nonmonotonic momentum dependence of the SC gap rather than the simplest $\Delta(\mathbf{k})\propto\cos(k_x a)-\cos(k_y a)$ d-wave form that well describes the gap function for p-doped cuprates with very tight Cooper pairs.[35,43]

IX. CONCLUSIONS

The superconducting (SC) phase diagram of the electron-doped cuprates has been explored by Raman spectroscopy. The SC gap magnitudes in optimally and overdoped samples are in agreement with the single particle spectroscopy measurements. The coupling decreases with increasing Ce concentrations from the strong-coupling regime for the underdoped sample to a weak-coupling regime at optimal doping and beyond. For the underdoped film, a collective mode in the Raman data in the SC state implies strong final state interactions. This collective mode appears in the B_{2g} channel in contrast to the p-doped cuprates where it appears in the B_{1g} channel. At this stage we can only stress the importance of this observation that has the potential of giving us an insight into the pairing mechanism in the SC state.[51,52] The full ramifications of this observation deserve further contemplation and are deferred to a later publication.

The persistence of SC coherence peaks in the B_{2g} channel for all dopings implies that superconductivity is mainly gov-

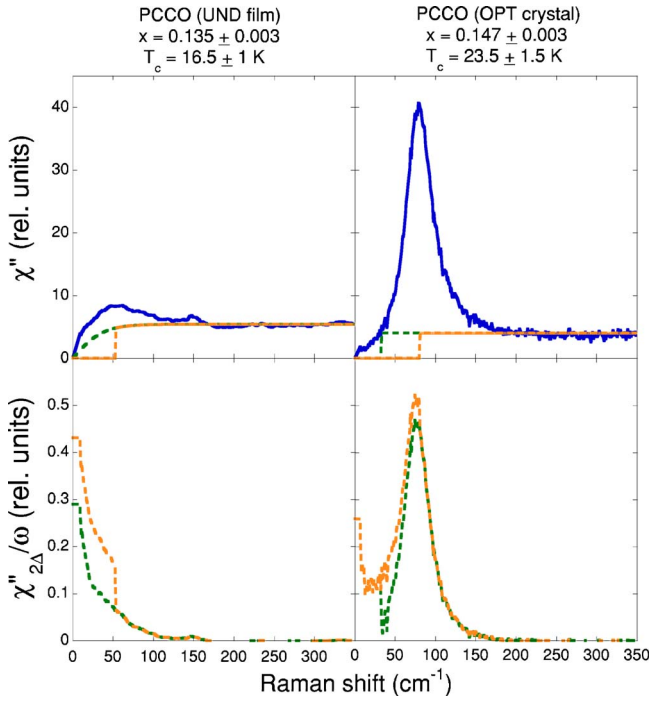

FIG. 8. (Color online) The panels show the main steps in computing $I_{SC}^{B_{2g}}(x)$ for underdoped PCCO (left column) and optimally doped PCCO (right column). The details about the different curves are given in the text.

erned by interactions in the vicinity of $(\pm\pi/2a, \pm\pi/2a)$ regions of the Brillouin zone. Moreover, the appearance of SC coherence as a collective mode in the B_{2g} channel in the underdoped sample ($x \approx 0.13$) coincides with the appearance of holelike carriers near $(\pm\pi/2a, \pm\pi/2a)$ regions of the BZ as seen by ARPES in underdoped NCCO.[8] For the sample with Ce doping $x \approx 0.13$, our B_{2g} Raman data show that SC pairing first occurs primarily near the $(\pm\pi/2a, \pm\pi/2a)$ regions of the BZ where holelike carriers reside while the more numerous electronlike carriers show no comparable sign of SC pairing in the B_{1g} channel. The presence of holelike carriers near $(\pm\pi/2a, \pm\pi/2a)$ regions of the BZ appears to be vital for superconductivity in the electron-doped cuprates.

Well-defined SC coherence peaks in the B_{1g} channel occur for optimally doped samples and this implies that the electronlike carriers near the $(\pm\pi/a, \pm\pi/4a)$ and $(\pm\pi/4a, \pm\pi/a)$ regions of the BZ are also gapped at this doping. Whether the pairing of electronlike carriers is driven by pairing of holelike carriers or occurs independently is an important question that requires further investigation.

Low energy scattering below the SC coherence peak energies for all dopings and Raman symmetries is most likely due to nodal QPs and means that the SC gap has nodes on the Fermi surface. This is consistent with phase sensitive measurements that find the SC pairing symmetry to be predominantly $d_{x^2-y^2}$.[16,72] However, the order parameter is likely to be more complicated than monotonic $d_{x^2-y^2}$[35,43,73] given the occurrence of two-band superconductivity and long SC coherence lengths.

We have also carried out a systematic spectroscopic study of magnetic field and temperature dependence of the electron-doped cuprates in the SC state. We have plotted the field and temperature dependence of the SC gap magnitude and the integrated intensity of the reduced 2Δ coherence peaks for various electron concentrations. From the temperature and doping dependence of the SC coherence peak, we extract an effective upper critical field line $H_{c2}^{*}(T,x)$ at which the superfluid stiffness vanishes. The field dependence of the measured SC gap reveals an estimate of $H_{c2}^{2\Delta}(T,x)$, an upper critical field at which the SC amplitude is completely suppressed by field. For optimally doped samples, the field effectively suppresses the superfluid stiffness while the SC amplitude survives higher fields suggesting a phase fluctuation regime for these samples. We find that magnetic field applied parallel to the c axis linearly suppresses the SC gap magnitude at a rapid rate, a phenomenon different from observations in other type-II superconductors in the clean limit.[59–61] This implies an unconventional pair-breaking mechanism for n-doped cuprates in a magnetic field.

We find that the SC coherence length, ξ_{SC} increases from 60 Å for optimal doping to 220 Å for the overdoped sample with $T_c = 13$ K. There appears to be a doping-dependent crossover in physical properties associated with superconductivity: relatively robust SC pairing at optimal doping becomes tenuous in the overdoped regime where field suppresses the pairing potential at an anomalously large rate while T_c still remains relatively high. We also find that carriers doped beyond optimal doping remain mainly incoherent and do not contribute to the Drude conductivity and superfluid density. This possibly explains the fragility of superconductivity in the overdoped regime of the electron-doped cuprates.

ACKNOWLEDGMENTS

The authors thank B. Liang, Y. Dagan, V. N. Kulkarni, Z. Y. Li, C. P. Hill, and M. Barr for assistance with preparation and characterization of samples. M.M.Q. and R.L.G. acknowledge the support of NSF Grant Nos. DMR 01-02350 and DMR 03-52735. C.A.K. acknowledges support from ONR/NRL.

APPENDIX

The panels in Fig. 8. show the main steps in the procedure for computing $I_{SC}^{B_{2g}}(x)$ for two doping concentrations of PCCO, underdoped PCCO in the left column, and optimally doped PCCO in the right column. The measured Raman response in the SC state at lowest temperature is depicted by solid blue (black) curves (at the lowest frequency, below 6 cm^{-1}, the data are linearly extrapolated to the $\omega \to 0$ limit). The orange (light gray) and green (dark gray) dashed lines in the upper two panels are the incoherent Raman continua based on two assumptions, respectively: (i) that the continuum vanishes just below 2Δ, and (ii) that it falls off at ω_c in the same way as it was derived from the fit to the data just above T_c. In the case of the optimally doped crystal, the scattering in the SC state falls off more rapidly at low frequencies than the continuum based on assumption (ii), and therefore the continuum is truncated at 30 cm^{-1}. The two

lower panels show $\chi''_{2\Delta}{}^{B_{2g}}/\omega$ after the continua are subtracted in two ways: orange (light gray) dashed curves, using assumption (i) and green (dark gray) dashed curves, for assumption (ii). The average of the areas under the two curves for each sample gives the value of the integrated intensity in the SC state and one-half the difference between the two areas was used as an estimate of the uncertainty. The same analysis was applied to the spectra from all other samples.

*Permanent address: University of California at San Diego, La Jolla, CA 92093.
†Permanent address: ISSMR, P.O. Box 270016, D-01171 Dresden, Germany.
‡Permanent address: Brookhaven National Laboratory, Upton, NY 11973.
§Corresponding author. Electronic address: girsh@bell-labs.com

[1] Z. Z. Wang, T. R. Chien, N. P. Ong, J. M. Tarascon, and E. Wang, Phys. Rev. B **43**, 3020 (1991).
[2] W. Jiang, S. N. Mao, X. X. Xi, X. Jiang, J. L. Peng, T. Venkatersan, C. J. Lobb, and R. L. Greene, Phys. Rev. Lett. **73**, 1291 (1994).
[3] P. Fournier, P. Mohanty, E. Maiser, S. Darzens, T. Venkatesan, C. J. Lobb, G. Czjzek, R. A. Webb, and R. L. Greene, Phys. Rev. Lett. **81**, 4720 (1998).
[4] P. Fournier, X. Jiang, W. Jiang, S. N. Mao, T. Venkatesan, C. J. Lobb, and R. L. Greene, Phys. Rev. B **56**, 14149 (1997).
[5] F. Gollnik and M. Naito, Phys. Rev. B **58**, 11734 (1998).
[6] Y. Dagan, M. M. Qazilbash, C. P. Hill, V. N. Kulkarni, and R. L. Greene, Phys. Rev. Lett. **92**, 167001 (2004).
[7] N. P. Armitage, F. Ronning, D. H. Lu, C. Kim, A. Damascelli, K. M. Shen, D. L. Feng, H. Eisaki, Z.-X. Shen, P. K. Mang, N. Kaneko, M. Greven, Y. Onose, Y. Taguchi, and Y. Tokura, Phys. Rev. Lett. **88**, 257001 (2002).
[8] H. Matsui, K. Terashima, T. Sato, T. Takahashi, S.-C. Wang, H.-B. Yang, H. Ding, T. Uefuji, and K. Yamada, Phys. Rev. Lett. **94**, 047005 (2005).
[9] D. van Harlingen, Rev. Mod. Phys. **67**, 515 (1995).
[10] C. C. Tsuei and J. R. Kirtley, Rev. Mod. Phys. **72**, 969 (2000).
[11] C. C. Tsuei, J. R. Kirtley, G. Hammerl, J. Mannhart, H. Raffy, and Z. Z. Li, Phys. Rev. Lett. **93**, 187004 (2004).
[12] A. Biswas, P. Fournier, M. M. Qazilbash, V. N. Smolyaninova, H. Balci, and R. L. Greene, Phys. Rev. Lett. **88**, 207004 (2002).
[13] J. A. Skinta, Min-Seog Kim, T. R. Lemberger, T. Greibe, and M. Naito, Phys. Rev. Lett. **88**, 207005 (2002).
[14] M. S. Kim, J. A. Skinta, T. R. Lemberger, A. Tsukada, and M. Naito, Phys. Rev. Lett. **91**, 087001 (2003).
[15] A. Snezhko, R. Prozorov, D. D. Lawrie, R. W. Giannetta, J. Gauthier, J. Renaud, and P. Fournier, Phys. Rev. Lett. **92**, 157005 (2004).
[16] Ariando, D. Darminto, H.-J. H. Smilde, V. Leca, D. H. A. Blank, H. Rogalla, and H. Hilgenkamp, Phys. Rev. Lett. **94**, 167001 (2005).
[17] T. Claesson, M. Mansson, C. Dallera, F. Venturini, C. De Nadai, N. B. Brookes, and O. Tjernberg, Phys. Rev. Lett. **93**, 136402 (2004).
[18] Y. Dalichaouch, B. W. Lee, C. L. Seaman, J. T. Markert, and M. B. Maple, Phys. Rev. Lett. **64**, 599 (1990).
[19] Y. Wang, S. Ono, Y. Onose, G. Gu, Y. Ando, Y. Tokura, S. Uchida, and N. P. Ong, Science **299**, 86 (2003).
[20] R. W. Hill, C. Proust, L. Taillefer, P. Fournier, and R. L. Greene, Nature (London) **414**, 711 (2001).
[21] H. Balci, C. P. Hill, M. M. Qazilbash, and R. L. Greene, Phys. Rev. B **68**, 054520 (2003).
[22] P. Fournier and R. L. Greene, Phys. Rev. B **68**, 094507 (2003).
[23] P. J. Hirschfeld and N. Goldenfeld, Phys. Rev. B **48**, 4219 (1993).
[24] H. Won and K. Maki, Phys. Rev. B **49**, 1397 (1994).
[25] B. S. Shastry and B. I. Shraiman, Phys. Rev. Lett. **65**, 1068 (1990).
[26] G. Blumberg and M. V. Klein, J. Low Temp. Phys. **117**, 1001 (1999).
[27] J. L. Peng, Z. Y. Li, and R. L. Greene, Physica C **177**, 79 (1991).
[28] E. Maiser, P. Fournier, J.-L. Peng, F. M. Araujo-Moreira, T. Venkatesan, R. L. Greene, and G. Czjzek, Physica C **297**, 15 (1998).
[29] J. L. Peng, E. Maiser, T. Venkatesan, R. L. Greene, and G. Czjzek, Phys. Rev. B **55**, R6145 (1997). Phys. Rev. Lett. **90**, 149702 (2003).
[30] S. B. Dierker, M. V. Klein, G. W. Webb, and Z. Fisk, Phys. Rev. Lett. **50**, 853 (1983).
[31] R. Hackl, R. Kaiser, and S. Schicktanz, J. Phys. C **16**, 1729 (1983).
[32] M. V. Klein and S. B. Dierker, Phys. Rev. B **29**, 4976 (1984).
[33] T. P. Devereaux and D. Einzel, Phys. Rev. B **51**, 16336 (1995).
[34] T. P. Devereaux, A. Virosztek, and A. Zawadowski, Phys. Rev. B **54**, 12523 (1996).
[35] G. Blumberg, A. Koitzsch, A. Gozar, B. S. Dennis, C. A. Kendziora, P. Fournier, and R. L. Greene, Phys. Rev. Lett. **88**, 107002 (2002).
[36] H. L. Liu, G. Blumberg, M. V. Klein, P. Guptasarma, and D. G. Hinks, Phys. Rev. Lett. **82**, 3524 (1999).
[37] T. Strohm and M. Cardona, Phys. Rev. B **55**, 12725 (1997).
[38] A. Koitzsch, G. Blumberg, A. Gozar, B. S. Dennis, P. Fournier, and R. L. Greene, Phys. Rev. B **67**, 184522 (2003).
[39] C. M. Varma, P. B. Littlewood, S. Schmitt-Rink, E. Abrahams, and A. E. Ruckenstein, Phys. Rev. Lett. **63**, 1996 (1989).
[40] The featureless continuum is stronger for the film samples compared to the single crystals. This is an indication of additional disorder and/or possible strain fields.
[41] T. P. Devereaux, D. Einzel, B. Stadlober, R. Hackl, D. H. Leach, and J. J. Neumeier, Phys. Rev. Lett. **72**, 396 (1994).
[42] T. P. Devereaux, Phys. Rev. Lett. **74**, 4313 (1995).
[43] H. Matsui, K. Terashima, T. Sato, T. Takahashi, M. Fujita, and K. Yamada, Phys. Rev. Lett. **95**, 017003 (2005).
[44] C. Kendziora, R. J. Kelley, and M. Onellion, Phys. Rev. Lett. **77**, 727 (1996).
[45] R. Hackl, G. Krug, R. Nemetschek, M. Opel, and B. Stadlober, Proc. SPIE Vol. **2696**, 194 (1996).
[46] T. Masui, M. Limonov, H. Uchiyama, S. Lee, S. Tajima, and A. Yamanaka, Phys. Rev. B **68**, 060506(R) (2003).
[47] M. M. Qazilbash, A. Biswas, Y. Dagan, R. A. Ott, and R. L. Greene, Phys. Rev. B **68**, 024502 (2003).
[48] G. Blumberg, M. Kang, M. V. Klein, K. Kadowaki, and C.

Kendziora, Science **278**, 1427 (1997).
[49] G. Blumberg, M. V. Klein, K. Kadowaki, C. Kendziora, P. Guptasarma, and D. Hinks, J. Phys. Chem. Solids **59**, 1932 (1998).
[50] A. Bardasis and J. R. Schrieffer, Phys. Rev. **121**, 1050 (1961).
[51] A. V. Chubukov, D. K. Morr, and G. Blumberg, Solid State Commun. **112**, 183 (1999).
[52] A. V. Chubukov, T. P. Devereaux, and M. V. Klein, cond-mat/0508643 (unpublished).
[53] A. Zimmers, R. P. S. M. Lobo, N. Bontemps, C. C. Homes, M. C. Barr, Y. Dagan, and R. L. Greene, Phys. Rev. B **70**, 132502 (2004).
[54] C. Kendziora and A. Rosenberg, Phys. Rev. B **52**, R9867 (1995).
[55] C. H. Choi and P. Muzikar, Phys. Rev. B **39**, 11296 (1989).
[56] Comparison of $I_{SC}^{B_{2g}}(x)$ with doping dependence of $1/\lambda^2$ is relevant if one assumes that the resonant properties of the Raman vertex, i.e., the optical conductivity near the laser excitation of 647 nm (1.9 eV), do not change with doping. Indeed, there is only a weak change in optical conductivity above 0.8 eV with doping in the relevant doping range ($0.13 < x < 0.18$) (Refs. 57 and 58).
[57] T. Arima, Y. Tokura, and S. Uchida, Phys. Rev. B **48**, 6597 (1993).
[58] Y. Onose, Y. Taguchi, K. Ishizaka, and Y. Tokura, Phys. Rev. B **69**, 024504 (2004).
[59] G. Blumberg, M. Kang, and M. V. Klein, Phys. Rev. Lett. **78**, 2461 (1997).
[60] R. Sooryakumar and M. V. Klein, Phys. Rev. Lett. **45**, 660 (1980).
[61] R. Sooryakumar and M. V. Klein, Phys. Rev. B **23**, 3213 (1981).
[62] A fit to the BCS theory does not necessarily mean that the gap in the over-doped samples has *s*-wave symmetry.
[63] Weak SC coherence peak intensity from the under-doped PCCO film makes it difficult to determine the gap values for higher fields. At present, we can only estimate the upper critical field H_{c2}^{*} at which the SC coherence peak vanishes.
[64] H. Balci and R. L. Greene, Phys. Rev. Lett. **93**, 067001 (2004).
[65] A. Biswas, P. Fournier, V. N. Smolyaninova, R. C. Budhani, J. S. Higgins, and R. L. Greene, Phys. Rev. B **64**, 104519 (2001).
[66] S. Kleefisch, B. Welter, A. Marx, L. Alff, R. Gross, and M. Naito, Phys. Rev. B **63**, 100507(R) (2001).
[67] L. Alff, Y. Krockenberger, B. Welter, M. Schonecke, R. Gross, D. Manske, and M. Naito, Nature (London) **422**, 698 (2003).
[68] Point contact tunneling (Ref. 47) gives a higher H_{c2} of 1.5 T for over-doped samples because the tunneling measurements were performed at a lower temperature (1.4 K).
[69] M. Tinkham, *Introduction to Superconductivity*, 2nd ed. (McGraw-Hill, New York, 1996).
[70] The higher H_{c2} estimates for over-doped samples extracted from resistivity and Nernst measurements may be due to T_c distribution in those samples (Refs. 21 and 22).
[71] N. P. Armitage, D. H. Lu, C. Kim, A. Damascelli, K. M. Shen, F. Ronning, D. L. Feng, P. Bogdanov, X. J. Zhou, W. L. Yang, Z. Hussain, P. K. Mang, N. Kaneko, M. Greven, Y. Onose, Y. Taguchi, Y. Tokura, and Z.-X. Shen, Phys. Rev. B **68**, 064517 (2003).
[72] C. C. Tsuei and J. R. Kirtley, Phys. Rev. Lett. **85**, 182 (2000).
[73] H. G. Luo and T. Xiang, Phys. Rev. Lett. **94**, 027001 (2005).